analytical chemistry

Article

pubs.acs.org/ac

Highly Sensitive Naphthalene-Based Two-Photon Fluorescent Probe for in Situ Real-Time Bioimaging of Ultratrace Cyclooxygenase-2 in Living Biosystems

Hua Zhang,*[,†] Jiangli Fan,[‡] Kui Wang,[†] Jing Li,[†] Caixia Wang,[†] Yamin Nie,[†] Tao Jiang,[†] Huiying Mu,[‡] Xiaojun Peng,[‡] and Kai Jiang[†]

[†]School of Chemistry and Chemical Engineering, Henan Normal University, 46 Jianshe Road, Muye Zone, Xinxiang 453007, P.R. China

[‡]State Key Laboratory of Fine Chemicals, Dalian University of Technology, 2 Linggong Road, Hi-Tech Zone, Dalian 116024, P.R. China

Supporting Information

ABSTRACT: Detecting and imaging of ultratrace cyclooxygenase-2 in living biosystems could provide much important valuable information for the diagnosis and intervention of cancer. Molecular probes, whose fluorescent signals are generated by cyclooxygenase-2, hold great potential for identification and enumeration of cyclooxygenase-2 in living biosystems. Although quite a few fluorescent probes have been reported for cyclooxygenase-2, the use fluorogenic probe with the excellent two-photon properties for the determination of ultratrace cyclooxygenase-2 has been scarce. Herein, an "off−on" fluorescence probe (**BTDAN-COX-2**), able to report and image the presence of ultratrace cyclooxygenase-2 in living biosystems, has been designed and evaluated. In order to improve sensitivity and specific selectivity of probe for ultratrace cyclooxygenase-2, **BTDAN-COX-2** employed cyclooxygenase-2's inhibitor as recognition group, because it is a classical and efficient recognition group for cyclooxygenase-2. A polarity-sensitive naphthalene derivative (**BTDAN**) as fluorophore was introduced into the molecule to enhance two-photon properties of **BTDAN-COX-2**. In the absent of cyclooxygenase-2, **BTDAN-COX-2** mainly exists in a folded conformation where probe fluorescence is quenched through photoinduced electron transfer between the fluorophore and the recognition group. Under the condition of existence of cyclooxygenase-2, fluorescence of probe is turned on, because photoinduced electron transfer between the fluorophore and the recognition group is restrained. **BTDAN-COX-2** provides high signal-to-background staining for the ultratrace cyclooxygenase-2 and has been successfully used to rapidly detect and image ultratrace cyclooxygenase-2 in living biosystems.

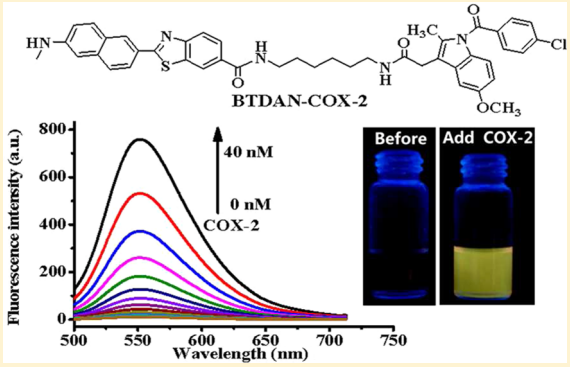

Cancer patients who were diagnosed in the early stage and subjected to surgery show far higher survival rates than those not subjected to surgery,[1−3] and therefore, the early diagnosis of cancer is critical to reversal and intervention of cancer development. Cyclooxygenase-2 (COX-2), an inducible enzyme, is an attractive target for the cancer early detection and imaging because it is associated with all stages of cancers from the earliest premalignancy phase to the later metastasis and diffusion.[4−6] Clinical data have thoroughly documented that COX-2 expression levels gradually increase from the ultratrace level to strong intensity during carcinogenic progression.[7−10] Accordingly, to develop the efficient, high-sensitivity methods for in situ real-time detection of the ultratrace COX-2 in living biosystems is of considerable significance for better diagnosing of cancer in the early stage.

Several traditional methods, for example, electrochemical analysis,[11] immunohistochemical method,[12] positron emission tomography[13,14] and single-photon emission computed tomography,[15,16] have been proposed for the detecting and imaging of COX-2 at trace quantity levels in various samples. These methods show high selectivity toward COX-2 and could meet the demands for the detection of COX-2 in solution and biological fluids. However, these methods are not appropriate for in situ real-time detection of COX-2 in living biosystems, because pretreatment processing, which may result in grave damage to living cell or tissues, are usually required before the detection and imaging.

By virtue of its higher sensitivity, real-time spatial high-resolution imaging, and the ability to safely examine (i.e., no or little damage) living biosystems in the detection and imaging process, two-photon fluorescence imaging technique[17−20] combined with active small molecular two-photon probes,

Received: May 25, 2014
Accepted: August 21, 2014
Published: August 21, 2014

   dx.doi.org/10.1021/ac501944y | *Anal. Chem.* 2014, 86, 9131−9138

presents exciting opportunities for in situ detection and imaging of specific diseases' marker molecules, for example, COX-2.[21−24] Recently, Marnett et al.[21,22] reported a series of exciting fluorescent probes for the detection and imaging of COX-2 in vivo and in vitro. In our previous work,[23,24] two cases of two-photon fluorescent probes for the imaging of COX-2 in living biosystems were developed, which were used to image Golgi of cancer cell and to discriminate cancer from inflammation, respectively. These works have widened the picture of possible molecular design ideas for the detecting and imaging of COX-2. However, the two-photon properties of these reported probes still need further optimization. Even more unfortunately, these reported probes are not suitable candidates for the detection and imaging of COX-2 in living biosystems at an ultratrace level.

In this work, we design and synthesize a new two-photon COX-2-specific fluorogenic probe, **BTDAN-COX-2** (Scheme 1), for specific COX-2 detection with improved sensitivity by employing a polarity sensitive naphthalene derivative as fluorophore and COX-2's inhibitor as recognition unit. **BTDAN-COX-2** is nonfluorescent in the absence of COX-2. And it shows "turned on" fluorescence enhancement as exposing to ultratrace COX-2 with obviously improved sensitivity, wider linear concentration range, and higher selectivity, compared with previous works.[23,24] Most importantly, it shows satisfactory sensitivity when it was applied to in situ real-time detecting and imaging of ultratrace COX-2.

EXPERIMENTAL SECTION

Reagents and Apparatus. All solvents and chemicals in this work were of analytical reagents. Column chromatographic purification used silica gel (200−300 mesh) as column chromatography packing. COX-2 was purchased from Sigma Chemical Co. (U.S.A.). Doubly purified water was used in all experiments. Mass spectrometric data were obtained on the LC/Q-TOF mass spectrometer. An auto sampler operated in-line with a quantum triple quadrupole instrument in ESI positive or negative ion mode. NMR spectra were recorded on the Varian Inova-400 MHz spectrometer. Experimental conditions were as follows: data matrix (2048 × 512), sweep width (13 ppm), recycles delay (1.5 s).

COX-2-Specific Fluorogenic Probe Synthesis. The synthetic procedures of **BTDAN-COX-2** and the intermediates are described in the Supporting Information (SI). **BTDAN-COX-2** and related intermediates were characterized by NMR and mass spectrometry, and its relevant spectra were described in SI.

Spectrophotometric Measurements. *Absorption and Fluorescence Quantum Yield Measurements.* A Lamda LS35 spectrophotometer (PerkinElmer, America) was used to obtain UV−vis absorption spectra. A FP-6500 spectrophotometer (Jasco, Japan) was used to measure the fluorescence spectra. Rhodamine B (Φ_F = 0.97 in methanol)[25] was used as a standard in the relative fluorescence quantum yields experiment. The relevant data were calculated by the following equation:

$$\Phi_x = \Phi_s(F_x/F_s)(A_s/A_x)(\lambda_{exs}/\lambda_{exx})(n_x/n_s)^2 \quad (1)$$

In this equation, Φ indicates the quantum yield; F represents the integrated area; absorbance at the excitation wavelength is expressed as A; the excitation wavelength is indicated as λ_{ex}; the refractive index of the solution is n; and the unknown and the standard indicate the subscripts x and s, respectively.

Fluorescence Responses to COX-2. The relevant two-photon fluorescence responses of probe **BTDAN-COX-2** (2.0 μM) to COX-2 (0−40 nM) in the Tris-HCl buffer (100 mM, pH = 8.0) were detected in spectral scanning mode by a laser scanning confocal microscope. The tunable filter was automatically stepped in 0.1 nm increments from 400 to 690 nm. The excitation light source was a mode-locked titanium-sapphire laser source (Coherent Chameleon, 90 MHz, 200 fs). The excitation wavelength was at 740 nm, and the output power was 1230 mW. Two-photon fluorescence spectra were sequentially obtained at each interval (0.5 nm). The fluorescence responses spectra of probe for COX-2 were captured by the ratio of fluorescence intensity (F/F_0) with the increasing amount of COX-2.

Measurement of Two-Photon Absorption Cross Section (δ). The femtosecond (fs) fluorescence measurement technique was used to detect the two-photon absorption cross section (δ) of the probe, which was described in the literature.[26] The probe, **BTDAN-COX-2**, was dissolved in different solvents at a concentration of 0.5 mM, and then the two-photon induced fluorescence intensity was obtained in the emission range of 500−600 nm under excitation at 690−920 nm. Fluorescein (0.8 μM, pH 11.0) was used as the reference.[27] The intensities of the two-photon induced fluorescence spectra of the reference and sample resulting from the same excitation wavelength were determined, respectively. δ was calculated by using eq 2:

$$\delta = \delta_r(S_s\Phi_r\varphi_r c_r)/(S_r\Phi_s\varphi_s c_s) \quad (2)$$

In this equation, the sample and reference molecules were expressed as the subscripts s and r. S denoted the intensity of the signal which was obtained by a CCD detector. Fluorescence quantum yield were expressed as Φ, and the overall fluorescence collection efficiency of the experimental apparatus were expressed as φ_t. In addition, c represented the concentration of the sample and reference molecules in solution, respectively. The measurements temperature were 25 ± 0.5 °C. The data were obtained from replicate experiments (n = 5). In the figure, $\Phi\delta$ as Y-axis and corresponding excitation wavelengths as X-axis were used, respectively.

Quantum Calculations. The Gaussian 09 suite was used to obtain all the data of quantum chemical calculations.[23,24,28,29] The density functional theory (DFT)[30] with Becke's three-parameter hybrid exchange function with Lee−Yang−Parr gradient-corrected correlation functional (B3-LYP functional) and 6-31G basis set used to perform the geometry optimizations of the dyes. No constraints to bonds/angles/dihedral angles were applied in the calculations, and all atoms were free to optimize. The electronic transition energies and corresponding oscillator strengths were calculated with time-dependent density functional theory (TD-DFT)[31,32] at the B3LYP/6-31G level.

Fluorescence Microscopy Imaging. *Cell Culture.* HeLa, MCF-7, and HEK293 cells were used in this work. Phenol red-free Dulbecco's Modified Eagle's Medium (DMEM, WelGene), which was added with penicillin/streptomycin and 10% fetal bovine serum (FBS; Gibco), was used to culture the HeLa, MCF-7, and HEK293 cells. Twenty-four hours before staining with dyes, cell lines were seeded into a glass-bottomed dish (MatTek, 35 mm dish with 20 mm well) and were cultured in a CO_2 (5 wt % /vol) incubator at 37 °C.

dx.doi.org/10.1021/ac501944y | Anal. Chem. 2014, 86, 9131−9138

Scheme 1. BTDAN, COX, and BTDAN-COX-2 (Folded and Unfolded)

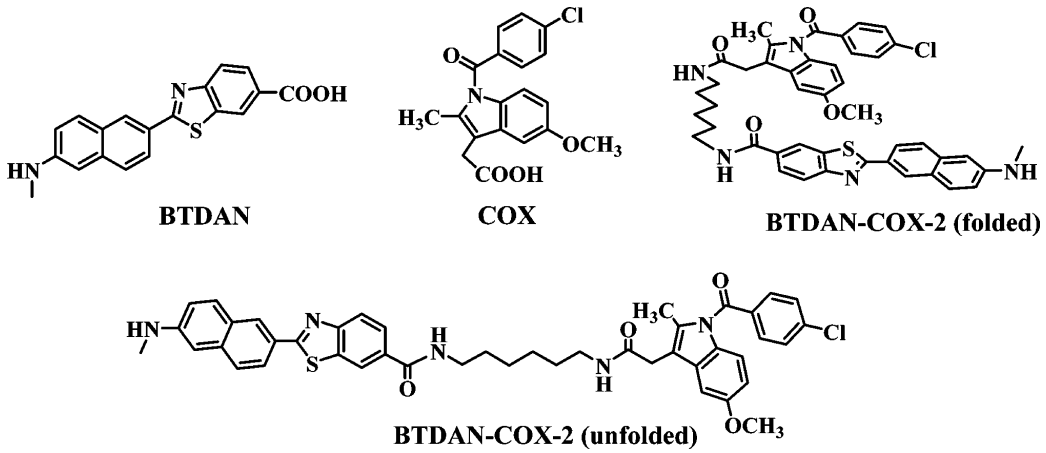

Tissue Slices Preparation. Tumor tissue slices were prepared from nude mice with S180 cancerous. The slices were cut at 800 μm using a vibrating-blade microtome in artificial cerebrospinal fluid (ACSF). ACSF was composed of 124 mM of NaCl, 3.00 mM of KCl, 26 mM of $NaHCO_3$, 1.25 mM of NaH_2PO_4, 10 mM of D-glucose, 2.40 mM of $CaCl_2$, and 1.30 mM of $MgSO_4$.

Staining. Concentrations of 2.0 μM and 30.0 μM **BTDAN-COX-2** were used to incubate live cells and tissues before imaging, respectively. They were incubated for 30 min at 37 °C under O_2/CO_2 (95%/5%), and then they were washed with phosphate-buffered saline (PBS) three times.

Fluorescence Imaging. The spectral confocal multiphoton microscope (Olympus, FV1000) with a high-performance mode-locked titanium-sapphire laser source (MaiTai, Spectra-Physics, U.S.A.) was used to obtain two-photon/one-photon fluorescence imaging in the cells and tissues. Numerical aperture (NA) was 1.43. Excitation wavelength was at 740 nm. The fluorescence intensity signals of BTDAN-COX-2 were collected in the range of 450−600 nm. The internal PMTs were used to obtain the intensity signal, which was installed as follow: 8 bit unsigned 1024 × 1024 pixels and 400 Hz scan speed. The intensity values of every image were collected from replicate experiments (n = 5).

Depth Imaging in Tissues. The changes of fluorescence intensity with scan depth were determined by spectral confocal multiphoton microscopy (Olympus, FV1000) in the z-scan mode from 0 to 700 μm. The step size in z-axis is 1.0 μm.

Fluorescence Imaging in Mice. **BTDAN-COX-2** (30 μL of 30 μM) were injected into the mice by tail vein. After being injected by **BTDAN-COX-2** for 30 min, the mice were imaged by the small animal in vivo imaging system (NightOWL II LB983, BERTHOLD TECHNOLOGIES). The excitation wavelength is at 488 nm. The fluorescence intensity signals are collected in the range of 550 ± 10 nm.

Cytotoxicity. MCF-7, Hela cells were prepared for cell viability studies (1 × 10^5 cells per well). The cells were incubated with dyes **BTDAN-COX-2** (5.0 μM) for 24 h. Subsequently, 100 μL of 3-(4,5-dimethylthiazol-2-yl)-2,5-diphenyltetrazolium bromide (MTT, Sigma Chemical Co. U.S.A.) was added into each well, and the cells were incubated for 4 h at 37 °C under O_2/CO_2 (95%/5%). The culture solution was removed. And then, to dissolve the reddish-blue crystals, 200 μL of DMSO (/well) was added into every well. Optical density (OD) was determined by a microplate reader (Spectra Max M5, Molecular Devices) at 570 nm with subtraction of the absorbance of the cell-free blank volume at 630 nm (n = 5). The relative cell viability (CV, 100%) was calculated using the following equation:

$$\mathrm{CV}(\%) = (\mathrm{OD}_{\mathbf{BTDAN\text{-}COX\text{-}2}} - \mathrm{OD}_{\mathbf{KBTDAN\text{-}COX\text{-}2}}) / (\mathrm{OD}_{\mathrm{control}} - \mathrm{OD}_{\mathrm{K\,control}}) \times 100 \quad (3)$$

Flow Cytometry. For flow cytometry studies, macrophages in the exponential phase of growth were plated into 35 mm glass-bottom culture dishes containing 2.0 mL of RPMI 1640. After incubation at 37 °C under O_2/CO_2 (95%/5%) for 1−2 days to reach 70−90% confluency, the medium was removed. Then the cells were washed with 2.0 mL of PBS buffer, and 2.0 mL of fresh RPMI 1640 was added along with iNOS stimulants. After incubation for 12 h, cells were taken to analyze by flow cytometry. Samples were illuminated with a sapphire laser at 488 nm on a FACS can flowcytometer (BD Biosciences Pharmingen, U.S.A.). The fluorescence of the forward-scattered and side-scattered light from 10 000 cells was detected at rate of 150 events/second. The data were analyzed with FACS Diva software.

Enzyme-Linked Immunosorbent Assay (ELISA). This assay used the ABC-double antibody sandwich ELISA method. COX-2 kit (human, double antibody method, 96t) was purchased from CBS. Cells and tissues were prepared as homogenates and preserved at 2−8 °C. According to literature procedures,[21] the ELISA assay experiment was carried out.

RESULTS AND DISCUSSION

Optimized Design and Synthesis of Two-Photon Probe for COX-2. Although quite a few small molecule fluorescent probes, including one-photon probes and two-photon probes, have been successfully developed for detecting and imaging of COX-2, there is not yet an excellent two-photon probe that can be used for ultratrace COX-2 detecting and imaging in living biosystems. Therefore, a core content of current work is to design a specific probe with high sensitivity and extraordinary two-photon properties for in situ real-time detecting and imaging of ultratrace COX-2. With this in mind, indomethacin (**COX**, Scheme 1) is used as recognition unit to specifically detect and image COX-2, because that **COX** could specific bond with the hydrophobic pocket of COX-2 which is comprised of Arg120, Tyr355, and Glu524.[21−24,33,34] Then, an acrylodan derivative, 6-(benzo[d]thiazol-2′-yl)-2-(*N*,*N*-dime-

dx.doi.org/10.1021/ac501944y | Anal. Chem. 2014, 86, 9131−9138

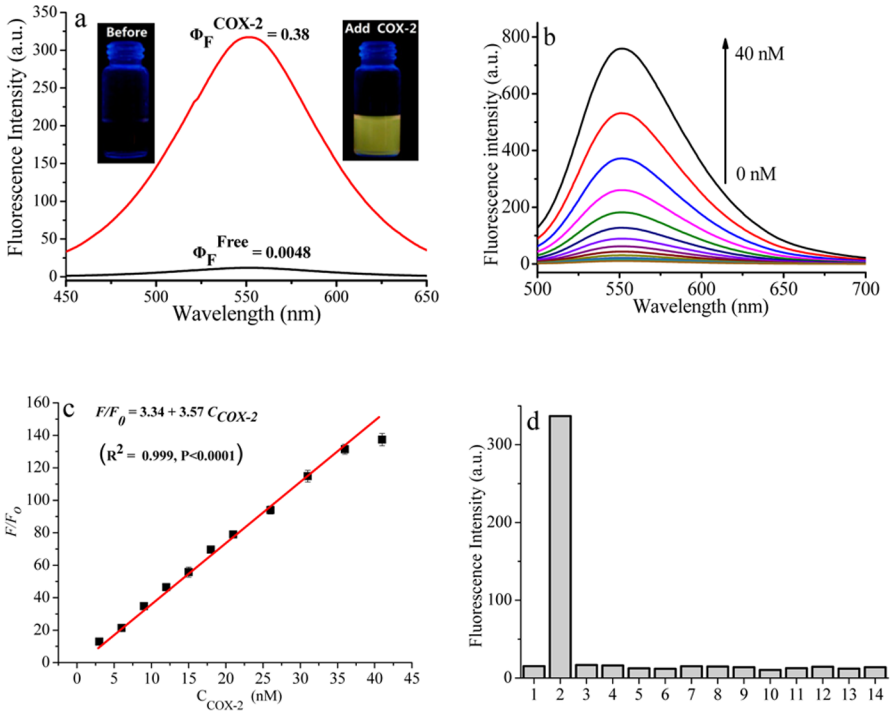

Figure 1. (a) Fluorescence spectra of **BTDAN-COX-2** (2.0 μM) in the absence and presence of COX-2 (20 nM) in buffer at 25 °C. (b) Fluorescence spectra of **BTDAN-COX-2** (2.0 μM) upon the concentrations of COX-2 increasing from 0 to 40 nM in Tris-HCl buffer (100 mM, pH 8.0). (c) The fluorescence of **BTDAN-COX-2** (2.0 μM) linear related to COX-2 concentration (1.0−36 nM). (d) Fluorescence changes with different biomolecules (0.050 μg/mL) in Tris-HCl buffer (100 mM, pH 8.0). 1, control; 2, COX-2; 3, COX-1; 4, DNA; 5, lysozyme; 6, triacylglycerol acylhydrolase; 7, histone; 8, proteinase k; 9, hemoglobin; 10, collagen; 11, β-amylase; 12, BSA; 13, trypsin; and 14, RNA.

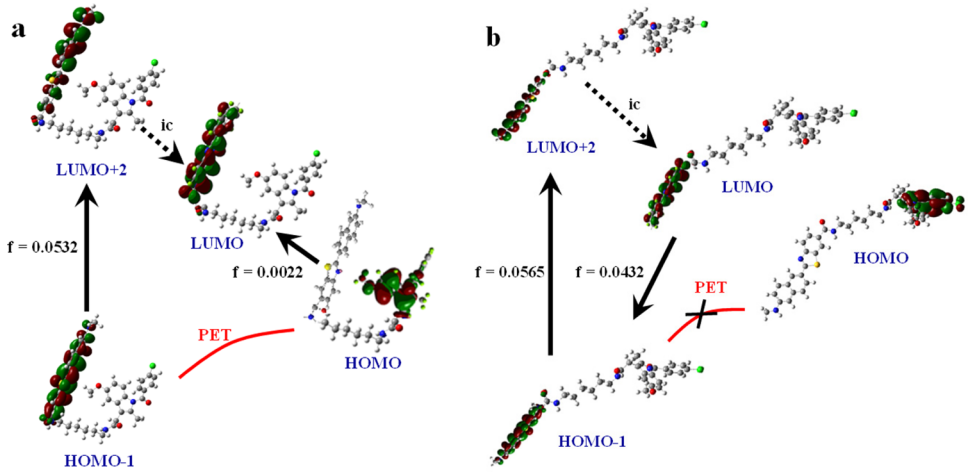

Figure 2. Structural optimization and Frontier molecular orbital (MO) of **BTDAN-COX-2**, both folded (a) and unfolded (b), calculated with time-dependent density functional theory using Gaussian 09.

thylamino) naphthalene (**BTDAN**, Scheme 1), was chosen as fluorophore to improve the probe's two-photon properties, considering its larger dipole moment at excitation state. More importantly, **BTDAN** is a hydrophobic molecule,[35−38] which allows it to easily enter the hydrophobic pocket of COX-2 and therefore increase the probe sensitivity.[21−24,33,34] Finally, a linear alkyl diamine was chosen as the linker which could form an amide bond with recognition unit **COX** at one end and a secondary amine bond with the fluorophore (**BTDAN**) at the other end. On the basis of our previous work,[23,24] we envisioned that such a design would give a molecule with specific selectivity, high sensitivity, and extraordinary two-photon properties to permit specific detecting and imaging ultratrace COX-2 in living biosystems.

The chemical structure and detailed synthetic route of **BTDAN-COX-2** and the key intermediates are described in SI (Scheme S1). The structures of **BTDAN-COX-2** and intermediates were well-characterized by ^{1}H NMR, ^{13}C NMR, and TOF-MS (see SI text).

Fluorescent Spectral Properties and Discussion of Mechanism. The fluorescent analytical performance of **BTDAN-COX-2** for COX-2 was analyzed in the Tris-HCl buffer (pH 8.0). The fluorescent data (Figure 1a) offered very encouraging signs that there was a significant fluorescence "off−on" process of **BTDAN-COX-2** when interacting with

dx.doi.org/10.1021/ac501944y | Anal. Chem. 2014, 86, 9131−9138

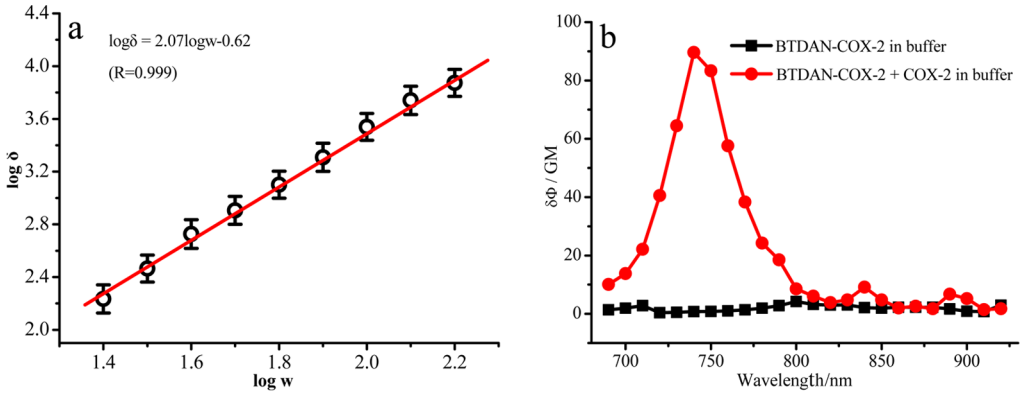

Figure 3. (a) Plot (log−log) of emission intensity against incident power. (b) Two-photon action spectra of **BTDAN-COX-2** (2.0 μM) in the absence (black curve) and presence (red curve) of COX-2 (13 nM) in Tris-HCl buffer (pH 8.0) at 25 °C. Data are from replicate experiments (n = 5).

ultratrace COX-2. When it was excited at 395 nm, **BTDAN-COX-2** (2.0 μM, ε = 15 700 M^{-1} cm^{-1}) is almost non-fluorescent in the absence of COX-2. However, it showed a 79-fold fluorescence enhancement at 550 nm arose within minutes upon binding to ultratrace COX-2 (C_{COX-2} = 20 nM, Φ_F^{Free} = 0.0048, Φ_F^{COX-2} = 0.38, Figure 1a). The large fluorescence enhancement together with almost zero background fluorescent of **BTDAN-COX-2** benefited with high sensitivity for target COX-2.

To elucidate the mechanism of the fluorescence "off−on" process between **BTDAN-COX-2** and COX-2, two low energy conformations of **BTDAN-COX-2** (namely, **BTDAN-COX-2-unfolded** and **BTDAN-COX-2-folded**, Scheme 1) were optimized by using Gaussian 09 (DFT/TDDFT in B3LYP/6-31G level), and their frontier molecular orbital energies in Tris-HCl buffer (pH 8.0) were calculated according to the reported method.[23,24] The calculated results indicated that the energy of the **BTDAN-COX-2-folded** (−1438327.6 kcal) was lower than that of **BTDAN-COX-2-unfolded** (−1438324.0 kcal), and its value was 3.6 kcal. This calculation indicated that unbounded **BTDAN-COX-2** exists mainly as the folded form (**BTDAN-COX-2-folded**) in the Tris-HCl buffer solution. Moreover, the oscillator strength of **BTDAN-COX-2-folded** in the Tris-HCl buffer for the electron transition from HOMO to LUMO is only 0.0022 (Figure 2a), which means that the electron transition from HOMO to LUMO is prohibited. So, the electronic transition from the excited state to the ground state cannot happen, and the fluorescence is quenched (Figure 2a). After binding of the **COX** moiety to COX-2, the probe could be force to adopt the unfolded conformation (**BTDAN-COX-2-unfolded**, Scheme 1), because the hydrophobic cavity of COX-2 only can hold the **COX** moiety.[23,24] As a result of the unfolding conformation, prohibited electron transition (PET) between **COX** and **BTDAN** did not occur (Figure 2b), therefore restoring fluorescence.[39]

The fluorescence spectra changes of **BTDAN-COX-2** upon the gradual addition of COX-2 are further investigated (Figure 1b). Upon the addition of COX-2, a gradually increasing fluorescence was observed at 550 nm, and its intensity increased linearly with the concentration of COX-2 ranging from 1.0 nM to 36 nM (Figure 1c). The detection limit of **BTDAN-COX-2** for COX-2 was experimentally determined to be about 1.0 nM, which is much lower than the previously reported COX-2 probe[21−24] Furthermore, this value is lower than the concentrations of COX-2 in cancer cells (30 nM), and higher than that in normal (0.08 nM) and inflammatory (0.91 nM).[24] So, it is favorable for direct imaging of intracellular ultratrace COX-2 in early stage of cancer. These results mentioned above indicated the success of our optimized design for the detecting of intracellular ultratrace COX-2 during early carcinogenic progression.

Besides sensitivity, selectivity is another crucial parameter to evaluate the performance of a new fluorescent probe for COX-2. Particularly, for the bioimaging probe with potential application in complex living biosystems, a specific response to the target specie over other potentially biological coexistence is a necessity. Therefore, the selectivity experiments of **BTDAN-COX-2** were extended to 13 kinds of other biological coexistences—biomolecules, such as COX-1, RNA, DNA, triacylglycerol acylhydrolase, BSA, and so on (Figure 1d). The specific responses of **BTDAN-COX-2** were found to be highly selective for COX-2 over other various biomolecules. Furthermore, **BTDAN-COX-2** did not exhibit observable fluorescence in the presence of COX-1, RNA, DNA, triacylglycerol acylhydrolase, BSA, and so on. IC_{50}, 50% inhibiting concentration of **BTDAN-COX-2** for biomolecules was used to evaluate the selective of **BTDAN-COX-2** for COX-2. The IC_{50} value of **BTDAN-COX-2** for COX-2 was 13.6 nM, which was far below those values of our previous two-photon COX-2 probes.[23,24] This result indicated the selectivity of **BTDAN-COX-2** for COX-2 was better than the reported probes in the previous works.[23,24] But, The IC_{50} values of **BTDAN-COX-2** for COX-1, RNA, DNA, triacylglycerol acylhydrolase, BSA were all larger than 75 mM, respectively, indicating that the selectivity of **BTDAN-COX-2** for COX-2 is much higher than that for COX-1, RNA, DNA, and triacylglycerol acylhydrolase. Moreover, experimental results indicated that **BTDAN-COX-2** was pH insensitive in the biologically relevant pH range (SI, Figure S1). All these results demonstrated that the probe, **BTDAN-COX-2**, is highly selective for COX-2 over other related biomolecules and could meet the selective requirements for bioimaging and detecting of intracellular ultratrace COX-2.

Two-Photon Fluorescence Properties of BTDAN-COX-2. Two-photon fluorescence microscopy imaging technology employing two near-infrared photons as the excitation source could offer a number of advantages over one-photon microscopy imaging technology, such as greater penetration depth into tissues, localization of excitation, longer observation time, and so on. In this work, **BTDAN-COX-2** can undergo a

dx.doi.org/10.1021/ac501944y | *Anal. Chem.* 2014, 86, 9131−9138

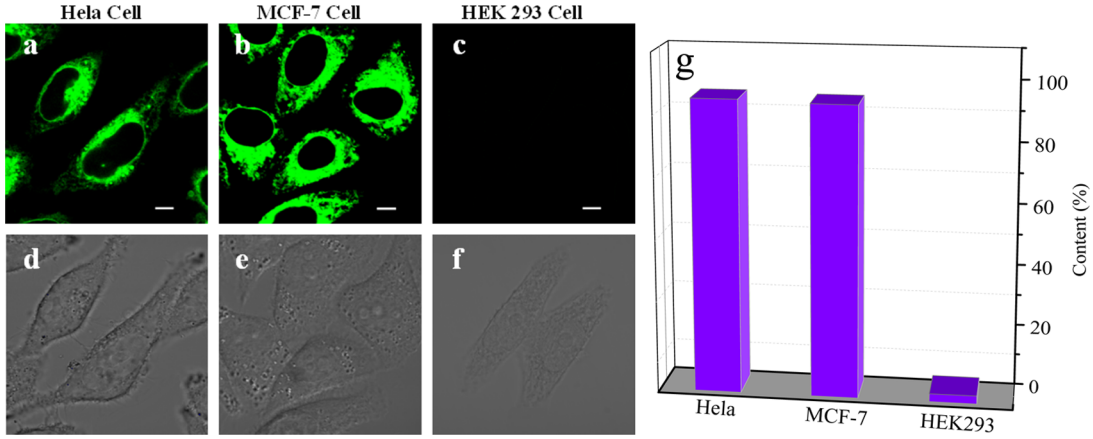

Figure 4. Living cells stained with **BTDAN-COX-2** (2.0 μM). (a–c) Fluorescence images. (d–f) White light images. (a,d) Hela cells. (b,e) MCF-7 cells; (c,f) HEK 293 cells. Excitation wavelength = 740 nm, scan range = 525–575 nm. Scale bar, 5.0 μm. (g) Data of flow cytometry (n = 5, p < 0.05); Images are representative of replicate experiments (n = 5).

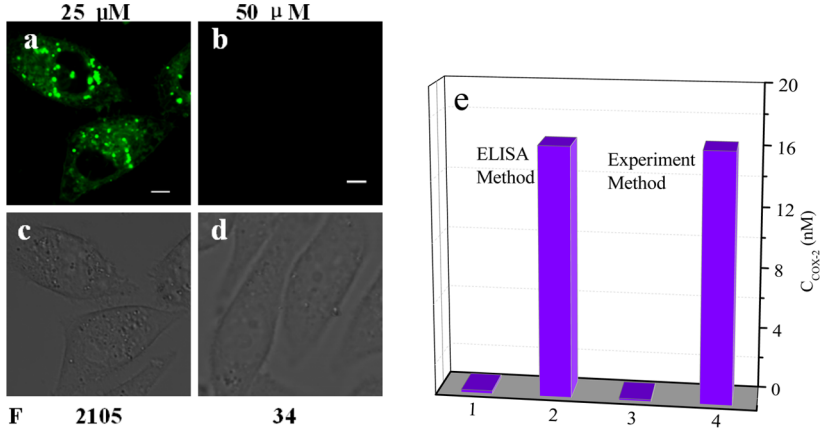

Figure 5. Quantitative detection of ultratrace COX-2 in live cells. Celecoxib of 25 and 50 μM were added in MCF-7 cells, respectively. (a,b) Fluorescence images; (c,d) White light images. **BTDAN-COX-2**: 2.0 μM; excitation wavelength: 740 nm; scan range: 525–575 nm; incubation time: 30 min; Scale bars: 5.0 μm. (e) Amount of COX-2 in Figure 5a,b (n = 5, p < 0.05). (1) Amount of COX-2 in Figure 5b was obtained by ELISA method; (2) Amount of COX-2 in Figure 5a was obtained by ELISA method; (3) Amount of COX-2 in Figure 5b was obtained by experiment method; (4) Amount of COX-2 in Figure 5a was obtained by experiment method.

two-photon excitation process, and this was confirmed by a power-dependence experiment (Figure 3). From the log–log plot of the emission intensity against incident power (Figure 3a), a linear regression with a slope of 2.07 was obtained, which is very close to 2, indicating an obvious two-photon excitation process.[40] The two-photon action cross section ($\Phi\delta$) is an important parameter for a two-photon probe. As shown in Figure 3b, the $(\Phi\delta)_{max}$ of **BTDAN-COX-2** is 90 GM (1GM = 10^{-50} cm^4 s/photon) when excited at 740 nm in the presence of COX-2 (13 nM). There was a 360-fold enhancement in the value $(\Phi\delta)_{max}$ compared with that seen in the absence of COX-2, which was much higher than that of the reported probes in the previous works.[23,24] These significant two-photon properties were due to **BTDAN-COX-2** as a polarity-sensitive naphthalene derivative appearing with a larger dipole moment at excitation state, which make **BTDAN-COX-2** suitable for two-photon fluorescence microscopy imaging COX-2 in living specimens at high resolution and sensitivity.[40,41]

Two-Photon Fluorescence Detecting and Imaging of BTDAN-COX-2 in Living Biosystems. **BTDAN-COX-2** shows a highly sensitive and selective response to ultratrace COX-2 and also a remarkable two-photon excited fluorescence enhancement induced by ultratrace COX-2 in Tris-HCl buffer (pH 8.0), which are especially favorable for two-photon fluorescence detecting and imaging of ultratrace COX-2 in living biosystems.

Before detecting and imaging, the toxicity and photostability of **BTDAN-COX-2** in living cells was investigated by MTT assay and two-photon fluorescence microscopy imaging, respectively. The MTT assay results (SI, Figure S2) revealed that greater than 90% of HeLa cells and MCF-7 cells survived after incubation with **BTDAN-COX-2** (2.0 μM) for 24 h. Even the incubation concentration of **BTDAN-COX-2** increased to 32 μM, greater than 85% of the cells still survived (SI, Figure S2). **BTDAN-COX-2** (2.0 μM) strongly stained cancer cells within 20 min, and that fluorescence intensity remained almost unchanged in cells for at least 7.0 h (SI Figure S3), which indicated that photostability of **BTDAN-COX-2** in cell imaging was better than that of our previous two-photon COX-2 probes.[23,24] The experiment results mentioned above showed that **BTDAN-COX-2** possesses very low cell toxicity and excellent photostability when it was once used for long-term detecting and imaging of COX-2 in living cells.

The specific selectivity of **BTDAN-COX-2** for COX-2 in living biosystems was then evaluated. **BTDAN-COX-2** (2.0 μM) showed the rapid and strong fluorescence responses to

dx.doi.org/10.1021/ac501944y | Anal. Chem. 2014, 86, 9131–9138

HeLa cells (Figure 4a) and MCF-7 cells (Figure 4b) which expressed COX-2. On the contrary, **BTDAN-COX-2** showed no such response to HEK 293 cells (Figure 4c) which almost did not express COX-2. Subsequently, flow cytometry (FCM) was used to evaluate the selectivity of **BTDAN-COX-2** for COX-2 on large cell populations. Histograms (Figure 4g) demonstrate that **BTDAN-COX-2** only stains HeLa cells and MCF-7 cells expressing COX-2, but it does not stain HEK 293 cells. All these results showed that **BTDAN-COX-2** exhibits satisfactory selectivity for COX-2 in living cells.

Imaging of ultratrace COX-2 in living biosystems could provide valuable information for the early diagnosis of cancer. In this experiment, a high affinity inhibitor, celecoxib, was selected to control the amount of COX-2 in cells at the ultratrace level, first. When 25 μM (Figure 5a) and 50 μM (Figure 5b) of celecoxib were delivered into MCF-7 cells, the fluorescence intensity of imaging decreased. The fluorescence intensity of Figure 5b was very weak, indicating that there was almost no COX-2. The results (Figure 5e) of ELISA method verified this conclusion. The average concentrations of COX-2 in Figure 5a estimated by the fluorescence intensity ratio (F/F_0) imaging method were 16.33 nM (Figure 5e and Figure 1c), which were consistent with the ELISA method (16.31 ± 0. 011 nM, $p < 0.05$).[42−44]

To investigate the applicability of this probe for ultratrace COX-2 detecting and imaging in tissues, the mouse S180 cancerous tissues in the early stage of carcinogenic progression were used for **BTDAN-COX-2** staining experiments. The results from fluorescence intensity ratio (F/F_0) imaging revealed that the average contents of COX-2 in early stage cancerous tissues were 10.57 nM (Figure 6a) and 17.19 nM (Figure 6b), respectively. These findings were consistent with the results obtained by the ELISA method (10.69 ± 0. 009 nM and 17.12 ± 0. 014 nM, $p < 0.05$, Figure 6c).[42−44]

To further assess **BTDAN-COX-2** as a two-photon fluorescent probe for bioimaging, this probe was used to depth image in tissue. After incubation of tissue slices (sarcoma 180) with 30.0 μM of **BTDAN-COX-2** for 30 min at 37 °C, two-photon images were obtained from 0 to 700 μm depth in the same region. Significantly, the tissue slices could be clearly visualized by green fluorescence at 30−430 μm depth (Figure 6d). All these results demonstrate that **BTDAN-COX-2** is membrane permeable and suitable for direct two-photon fluorescent depth imaging of ultratrace COX-2 in tissues.

The probe's potential for in vivo imaging was evaluated using carrageenan-induced ultratrace COX-2 in the mouse foot. The mouse foot model is well-documented for the role of ultratrace COX-2-derived prostaglandins as a major driving force for the acute edema that results 24 h after carrageenan injection into the paw.[45] For comparison, mouse without carrageenan-induced COX-2 were also dosed with **BTDAN-COX-2**. Both mice were imaged at 30 min postinjection. In Figure 7a, there was almost nonfluorescent, but, it showed obvious fluorescent in Figure 7b. The result indicates the probe had selectively accumulated in ultratrace COX-2 in vivo.

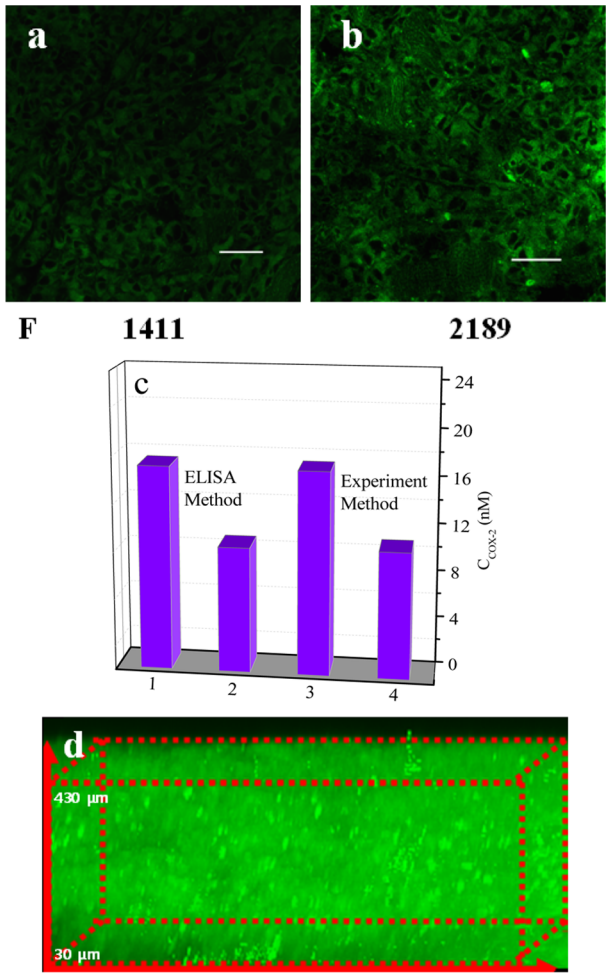

Figure 6. Quantitative detection of ultratrace COX-2 in tissues. (a,b) Fluorescence images; **BTDAN-COX-2**: 20.0 μM; excitation wavelength: 740 nm; scan range: 525−575 nm; incubation time: 30 min; Scale bars: 30.0 μm. (c) Amount of COX-2 in Figure 6a and b ($n = 5$, $p < 0.05$). (1) The amount of COX-2 in Figure 6b was obtained by ELISA method; (2) Amount of COX-2 in Figure 6a was obtained by ELISA method; (3) Amount of COX-2 in Figure 6b was obtained by experiment method; (4) Amount of COX-2 in Figure 6a was obtained by experiment method. (d) Depth imaging of **BTDAN-COX-2** (30.0 μM) in tissue. Images were generated using excitation by the two-photon lasers at 740 nm and were collected at 525−575 nm.

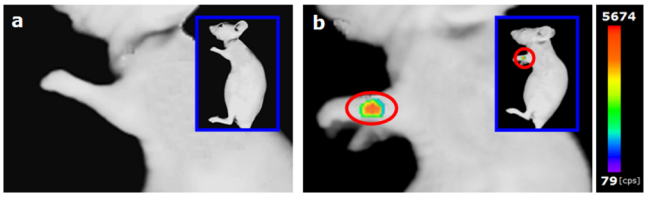

Figure 7. In vivo labeling of ultratrace COX-2 by probe **BTDAN-COX-2** (30 μL of 30 μM). Mouse with carrageenan-induced inflammation in the left foot. Panel a was not induced with the carrageenan. Panel b was induced with the carrageenan. Both mice were imaged at 30 min postinjection.

CONCLUSIONS

We exploited the flexibility of the COX-2 substrate-specificity loop by attaching naphthalene derivative to indomethacin to form **BTDAN-COX-2**. The fluorescence of **BTDAN-COX-2** with form of **BTDAN-COX-2-folded** is quenched in the absence of COX-2. Intriguingly, the fluorescence of **BTDAN-COX-2** is "turned on" in solution, cells, and tissues where COX-2 merely expressed at ultratrace level. The generated fluorescent signal for the ultratrace COX-2 results from restraining of PET after **BTDAN-COX-2** binding to COX-2, and the sensibility of naphthalene derivative for hydrophobic environment of COX-2, which affords a high sensitivity to

dx.doi.org/10.1021/ac501944y | Anal. Chem. 2014, 86, 9131−9138

COX-2 with a detection limit 1.0 nM observed, much lower than the previously reported COX-2-probe. **BTDAN-COX-2** exhibits a high selectivity for ultratrace COX-2 over other biological species tested including COX-1. Furthermore, the push−pull charge-transfer structure of **BTDAN-COX-2** provides significant two-photon properties for the imaging in biosystem. All these features enable **BTDAN-COX-2** more favorable for direct monitoring of ultratrace COX-2 in biosystem at the early stage of cancer, compared with our previously reported probes.[23,24] It was then successfully applied to direct two-photon plane and depth imaging ultratrace COX-2 in mouse S180 cancerous tissues and in vivo, demonstrating its value of practical application at the early diagnosis of cancer.

■ ASSOCIATED CONTENT

Ⓢ Supporting Information

Additional information as noted in text. Supporting Information is available free of charge via the Internet at http://pubs.acs.org.

■ AUTHOR INFORMATION

Corresponding Author

*Email: zhanghua1106@163.com. Tel/Fax: +86-373-3329030.

Author Contributions

All authors have given approval to the final version of the manuscript.

Notes

The authors declare no competing financial interest.

■ ACKNOWLEDGMENTS

This work was financially supported by NSF of China (nos. 21136002, 21376039, 21402043, and 61176004).

■ REFERENCES

(1) Greenlee, R. T.; Murray, T.; Bolden, S.; Wingo, P. A. *Cancer. J. Clin.* **2000**, *50*, 7−33.
(2) Crofford, L. J. *J. Rheumatol.* **1997**, *49*, 15−19.
(3) Dannenberg, A. J.; Lippman, S. M.; Mann, J. R.; Subbaramaiah, K.; DuBois, R. N. *J. Clin. Oncol.* **2005**, *23*, 254−266.
(4) Crofford, L. J. *J. Rheumatol.* **1997**, *49*, 15−19.
(5) Dannenberg, A. J.; Lippman, S. M.; Mann, J. R.; Subbara-maiah, K.; DuBois, R. N. J. *Clin. Oncol.* **2005**, *23*, 254−266.
(6) Subbaramaiah, K.; Dannenberg, A. J. *Trends. Pharmacol. Sci.* **2003**, *24*, 96−102.
(7) Kandil, H. M.; Tanner, G.; Smalley, W.; Halter, S.; Radhika, A.; Dubois, R. N. *Dig. Dis. Sci.* **2001**, *46*, 785−789.
(8) Eberhart, C. E.; Coffey, R. J.; Radhika, A.; Giardiello, F. M.; Ferrenbach, S.; DuBois, R. N. *Gastroenterology* **1994**, *107*, 1183−1188.
(9) Kargman, S. L.; O'Neill, G. P.; Vickers, P. J.; Evans, J. F.; Mancini, J. A.; Jothy, S. *Cancer. Res.* **1995**, *55*, 2556−2559.
(10) Soslow, R. A.; Dannenberg, A. J.; Rush, D.; Woerner, B. M.; Khan, K. N.; Masferrer, J.; Koki, A. T. *Cancer* **2000**, *89*, 2637−2645.
(11) Noah, N. M.; Marcells, O.; Almalleti, A.; Lim, J.; Sadik, O. A. *Electroanalysis* **2011**, *23*, 2392−2399.
(12) Mendes, R. A.; Carvalho, J. F. C.; van der Waal, I. *J. Oral Pathol. Med.* **2011**, *40*, 497−503.
(13) Prabhakaran, J.; Underwood, M. D.; Parsey, R. V.; Arango, V.; Majo, V. J.; Simpson, N. R.; Heertum, R. V.; Mann, J. J.; Dileep Kumar, J. S. *Bioorg. Med. Chem.* **2007**, *15*, 1802−1807.
(14) Wuest, F.; Kniess, T.; Bergmann, R.; Pietzsch, J. *Bioorg. Med. Chem.* **2008**, *16*, 7662−7670.
(15) Vries, E. F.; Waarde, A.; Buursma, A. R.; Vaalburg, W. *J. Nucl. Med.* **2003**, *44*, 1700−1706.
(16) Tanaka, M.; Fujisaki, Y.; Kawamura, K.; et al. *Biol. Pharm. Bull.* **2006**, *29*, 2087−2094.
(17) Que, E. L.; Domaille, D. W.; Chang, C. *J. Chem. Rev.* **2008**, *108*, 1517−1549.
(18) Thoumine, O.; Ewers, H.; Heine, M.; Groc, L.; Frischknecht, R.; Giannone, G.; Poujol, C.; Legros, P.; Lounis, B.; Cognet, L.; Choquet, D. *Chem. Rev.* **2008**, *108*, 1565−1587.
(19) Yang, Y. M.; Zhao, Q.; Feng, W.; Li, F. Y. *Chem. Rev.* **2013**, *112*, 192−270.
(20) Kim, H. M.; Cho, B. R. *Acc. Chem. Res.* **2009**, *42*, 863−872.
(21) Uddin, M. J.; Crews, B. C.; Blobaum, A. L.; Kingsley, P. J.; Gorden, D. L.; McIntyre, J. O.; Matrisian, L. M.; Subbaramaiah, K.; Dannenberg, A. J.; Piston, D. W.; Marnett, L. J. *Cancer Res.* **2010**, *70*, 3618−3627.
(22) Uddin, M. J.; Crews, B. C.; Ghebreselasie, K.; Marnett, L. J. *Bioconjugate Chem.* **2013**, *24*, 712−723.
(23) Zhang, H.; Fan, J. L.; Wang, J. Y.; Zhang, S. Z.; Dou, B. R.; Peng, X. J. *J. Am. Chem. Soc.* **2013**, *135*, 11663−11669.
(24) Zhang, H.; Fan, J. L.; Wang, J. Y.; Dou, B. R.; Zhou, F.; Cao, J. F.; Qu, J. L.; Cao, Z.; Zhao, W. J.; Peng, X. J. *J. Am. Chem. Soc.* **2013**, *135*, 17469−17475.
(25) Velapoldi, R. A.; T€onnesen, H. H. *J. Fluoresc.* **2004**, *14*, 465−472.
(26) Lee, S. K.; Yang, W. J.; Choi, J. J.; Kim, C. H.; Jeon, S. J.; Cho, B. R. *Org. Lett.* **2005**, *7*, 323−326.
(27) Xu, C.; Webb, W. W. *J. Opt. Soc. Am. B* **1996**, *13*, 481−489.
(28) Frisch, E.; Frisch, M. J.; Clemente, F. R.; Trucks, G. W. *Gaussian 09*, revision A.02; Gaussian, Inc.: Wallingford, CT, 2009.
(29) Zhou, L. C.; Zhao, G. J.; Liu, J. F.; Han, K. L.; Wu, Y. K.; Peng, X. J.; Sun, M. T. *J. Photochem. Photobiol. A: Chemistry* **2007**, *187*, 305−310.
(30) Dreizler, M. R.; Gross, E. K. U. *Density Functional Theory*; Springer Verlag: Heidelberg, 1990.
(31) Gross, E. K. U.; Kohn, W. *Phys. Rev. Lett.* **1985**, *55*, 2850−2852.
(32) Stratmann, R. E.; Scuseria, G. E.; Frisch, M. J. *J. Chem. Phys.* **1998**, *109*, 8218−8224.
(33) Bhattacharyya, D. K.; Lecomte, M.; Rieke, C. J.; Garavito, R. M.; Smith, W. L. *J. Biol. Chem.* **1996**, *271*, 2179−2184.
(34) Kalgutkar, A. S.; Crews, B. C.; Rowlinson, S. W.; Marnett, A. B.; Kozak, K. R.; Remmel, R. P.; Marnett, L. J. *Proc. Natl. Acad. Sci. U.S.A.* **2000**, *97*, 925−930.
(35) Lim, C. S.; Masanta, G.; Kim, H. J.; Han, J. H.; Kim, H. M.; Cho, B. R. *J. Am. Chem. Soc.* **2011**, *133*, 11132−11135.
(36) Bae, S. K.; Heo, C. H.; Choi, D. J.; Sen, D.; Joe, E. H.; Cho, B. R.; Kim, H. M. *J. Am. Chem. Soc.* **2013**, *135*, 9915−9923.
(37) Masanta, G.; Heo, C. H.; Lim, C. S.; Bae, S. K.; Cho, B. R.; Kim, H. M. *Chem. Commun.* **2012**, *48*, 3518−3520.
(38) Baek, N. Y.; Heo, C. H.; Lim, C. S.; Masanta, G.; Cho, B. R.; Kim, H. M. *Chem. Commun.* **2012**, *48*, 4546−4548.
(39) Zhang, X.; Wu, Y. B.; Ji, S. M.; Guo, H. M.; Song, P.; Han, K. L.; Wu, W. T.; Wu, W. H.; James, T. D.; Zhao, J. Z. *J. Org. Chem.* **2010**, *75*, 2578−2588.
(40) Xu, C.; Zipfel, W.; Shear, J. B.; Williams, R. M.; Webb, W. W. *Proc. Natl. Acad. Sci. U.S.A.* **1996**, *93*, 10763−10768.
(41) Xu, C.; Webb, W. W. *J. Opt. Soc. Am. B* **1996**, *13*, 481−491.
(42) Tucker, O. N.; Dannenberg, A. J.; Yang, E. K.; Zhang, F.; Teng, L.; Daly, J. M.; Soslow, R. A.; Masferrer, J. L.; Woerner, B. M.; Koki, A. T.; Fahey, T. J. *Cancer Res.* **1999**, *59*, 987−990.
(43) Eberhart, C. E.; Coffey, R. J.; Radhika, A.; Giardiello, F. M.; Ferrenbach, S.; Dubois, R. N. *Gastroenterology* **1994**, *107*, 1183−1188.
(44) Samad, T. A.; Moore, K. A.; Sapirstein, A.; Billet, S.; Allchorne, A.; Poole, S.; Bonventre, J. V.; Woolf, C. J. *Nature* **2001**, *410*, 471−475.
(45) di Meglio, P.; Ianaro, A.; Ghosh, S. *Arthritis Rheum.* **2005**, *52*, 951−958.